Developmental Changes in P-Glycoprotein Function in the Blood–Brain Barrier of Nonhuman Primates: PET Study with *R*-^{11}C-Verapamil and ^{11}C-Oseltamivir

Tadayuki Takashima[1], Chihiro Yokoyama[1], Hiroshi Mizuma[1], Hajime Yamanaka[1], Yasuhiro Wada[1], Kayo Onoe[1], Hiroko Nagata[1], Shusaku Tazawa[1], Hisashi Doi[1], Kazuhiro Takahashi[1], Masataka Morita[2], Motomu Kanai[2], Masakatsu Shibasaki[2], Hiroyuki Kusuhara[2], Yuichi Sugiyama[2], Hirotaka Onoe[1], and Yasuyoshi Watanabe[1]

[1]*RIKEN Center for Molecular Imaging Science, Chuo-ku, Kobe, Japan; and* [2]*Graduate School of Pharmaceutical Sciences, the University of Tokyo, Hongo, Bunkyo-ku, Tokyo, Japan*

P-glycoprotein (P-gp) plays a pivotal role in limiting the penetration of xenobiotic compounds into the brain at the blood–brain barrier (BBB), where its expression increases with maturation in rats. We investigated developmental changes in P-gp function in the BBB of nonhuman primates using PET with *R*-^{11}C-verapamil, a PET radiotracer useful for evaluating P-gp function. In addition, developmental changes in the brain penetration of ^{11}C-oseltamivir, a substrate for P-gp, was investigated as practical examples. **Methods:** PET studies in infant (age, 9 mo), adolescent (age, 24–27 mo), and adult (age, 5.6–6.6 y) rhesus monkeys (*Macaca mulatta*) were performed with *R*-^{11}C-verapamil and also with ^{11}C-oseltamivir. Arterial blood samples and PET images were obtained at frequent intervals up to 60 min after administration of the PET tracer. Dynamic imaging data were evaluated by integration plots using data collected within the first 2.5 min after tracer administration. **Results:** *R*-^{11}C-verapamil rapidly penetrated the brain, whereas the blood concentration of intact *R*-^{11}C-verapamil decreased rapidly in all subjects. The maximum brain uptake in infant (0.033% ± 0.007% dose/g of brain) and adolescent (0.020% ± 0.002% dose/g) monkeys was 4.1- and 2.5-fold greater, respectively, than uptake in adults (0.0082% ± 0.0007% dose/g). The clearance of brain *R*-^{11}C-verapamil uptake in adult monkeys was 0.056 ± 0.010 mL/min/g, significantly lower than that in infants (0.11 ± 0.04 mL/min/g) and adolescents (0.075 ± 0.023 mL/min/g). ^{11}C-oseltamivir showed little brain penetration in adult monkeys, with a clearance of *R*-^{11}C-verapamil uptake of 0.0072 and 0.0079 mL/min/g, slightly lower than that in infant (0.0097 and 0.0104 mL/min/g) and adolescent (0.0097 and 0.0098 mL/min/g) monkeys. **Conclusion:** These results suggest that P-gp function in the BBB changes with development in rhesus monkeys, and this change may be closely related to the observed difference in drug responses in the brains of children and adult humans.

Key Words: positron emission tomography; blood-brain barrier; P-glycoprotein; developmental change; rhesus monkey

J Nucl Med 2011; 52:950–957
DOI: 10.2967/jnumed.110.083949

Drug dosage regimen design and toxicologic assessment in children remain significant challenges in clinical care and environmental risk assessment because of the influence of ontogeny on drug disposition (*1*). Some drug-metabolizing enzymes display ontogeny (*2,3*) in humans, but the ontogeny of drug transporters has been described only in murine models.

The blood–brain barrier (BBB) restricts the entry of circulating drugs and xenobiotics into the brain, and thus the action of drugs in the central nervous system (CNS) depends on their systemic circulation and their ability to permeate the BBB. In the BBB, highly developed tight junctions between adjacent brain capillary endothelial cells act as a diffusion barrier. Metabolic enzymes and active efflux transporters for specific compounds are also located here (*4,5*). The formation of tight junctions is completed before birth, and mice lacking the tight junction protein claudin-5 die within 10 h of birth (*6*). Expression of the efflux transporter P-glycoprotein (P-gp) in the BBB, however, increases with age in rats (*7,8*).

P-gp is a 170-kDa membrane adenosine triphosphate–binding cassette efflux transporter encoded by the multidrug resistance 1 (rodents, *Mdr1a* or *Mdr1b;* humans, *MDR1*) gene (*9,10*). Numerous studies have revealed that P-gp limits the penetration of a variety of compounds into the brain by extruding them into the blood on the luminal membrane of brain capillary endothelial cells, thereby attenuating the pharmacologic action of drugs in the brain (*11,12*). Impairment of P-gp by gene mutation or inhibition of P-gp by drug–drug interaction sensitizes mice to ivermectin, morphine-6-glucuronide, and dasatinib and also sensitizes dogs to ivermectin, vincristine, vinblastine, and doxorubicin (*13–15*). Lopera-

Received Oct. 12, 2010; revision accepted Feb. 16, 2011.
For correspondence or reprints contact: Hirotaka Onoe, Functional Probe Research Laboratory, RIKEN Center for Molecular Imaging Science, 6-7-3 Minatojima, Minamimachi, Chuo-ku, Kobe, Hyogo 650-0047, Japan.
E-mail: hiro.onoe@riken.jp

mide coadministered with the P-gp inhibitor quinidine reportedly causes respiratory depression, a CNS effect of opioids, presumably because of P-gp inhibition by quinidine (*16*). Thus, the changes in P-gp expression level in the brain may affect the brain concentration of P-gp substrates such as cyclosporine A and digoxin. Brain expression of *Mdr1a* P-gp, a predominant isoform in the BBB, is lower at the messenger RNA level in newborn rats on postnatal days 1–11 and lower at the protein level in newborn rats (postnatal days 1–7) and infant rodents (postnatal day 14) than in adult rats (postnatal days 42 and beyond) (*7,8*). It was reported that when loperamide, a P-gp substrate, was administered to young children as a drug for diarrhea, opiatelike side effects in the CNS were observed (*17*). Therefore, there is growing interest in how P-gp is expressed in the BBB during human development; a more thorough understanding of developmental changes in P-gp function in the BBB would greatly improve the ability to predict therapeutic benefits and potential risks associated with drug treatments in children.

The present study investigated P-gp function in the BBB in infant, adolescent, and adult nonhuman primates using PET. PET allows direct measurement of the brain concentration of administered radiotracer at multiple time points, with high sensitivity and spatial-temporal resolution, and has already been used for in vivo functional analysis of BBB-associated P-gp.

Among numerous ^{11}C-labeled P-gp substrates, ^{11}C-verapamil has been well characterized (*18–20*). Cyclosporine A and its analog significantly increase clearance of ^{11}C-verapamil in the brain of monkeys and healthy humans (*19,21*). ^{11}C-verapamil has been used to investigate variations in P-gp function at the BBB caused by single-nucleotide polymorphisms (*22*) and by Parkinson disease (*23*). We used *R*-^{11}C-verapamil, an enantiomer of ^{11}C-verapamil, as a probe for P-gp. Although there are no stereoselectivity effects in the transport of *R*- and *S*-verapamil by P-gp (*18*), *R*-^{11}C-verapamil has several advantages over *S*-^{11}C-verapamil, including a lower affinity for calcium channels and a lower metabolism in humans (*24*). Several reports showed that ^{11}C-verapamil is also a sensitive probe for BBB P-gp activity in nonhuman primates (*19,25–27*).

Oseltamivir, an antiviral drug, has been reported to be a substrate of P-gp. Although the brain penetration of oseltamivir in primates has not been elucidated yet, its abnormal behavior in children is suspected to be due to CNS effects (*28*). Recently, Morita et al. (*29*) have reported on a procedure for the synthesis of ^{11}C-oseltamivir for the application to ^{11}C-oseltamivir PET in higher animals such as monkeys. Understanding of developmental changes in brain penetration of oseltamivir together with that in P-gp function would explain one of the causes of suspected aversive central effects in children. Therefore, in the present study, we also examined changes in brain penetration of ^{11}C-oseltamivir during development as practical examples with the same monkeys used in ^{11}C-verapamil study, to better understand the age-dependent adverse effects of ^{11}C-oseltamivir.

MATERIALS AND METHODS

Radiolabeled Probes

^{11}C-labeled *R*-verapamil was prepared from *R*-norverapamil (Advanced Biochemical Compounds), with slight modifications of previously described procedures for preparing racemic ^{11}C-verapamil (*30*). ^{11}C-labeled oseltamivir was prepared from its deacetylated derivative according to previously described procedures (*29*). Purified fractions of each compound were evaporated and reconstituted with approximately 5 mL of saline solution. The specific radioactivity was 55 ± 34 GBq/μmol and 46 ± 6 GBq/μmol for *R*-^{11}C-verapamil and ^{11}C-oseltamivir, respectively. The radiochemical purity and chemical purity of both compounds was higher than 98% at the time of synthesis.

Animals

Male rhesus monkeys (*Macaca mulatta*) weighing 1.4–1.9 kg (infant; age, 9 mo, $n = 5$), 2.0–2.6 kg (adolescent; age, 24–27 mo, $n = 5$), and 5.7–7.8 kg (adult; age, 5.6–6.6 y, $n = 5$) were used for the *R*-^{11}C-verapamil study. Two of the 5 animals from each age group were also used in the ^{11}C-oseltamivir PET study. Monkeys were maintained and handled in accordance with recommendations of the Center for Molecular Imaging Science, RIKEN Ethics Committee on Animal Care and Use. PET experiments were performed in accordance with the *Guide for the Care and Use of Laboratory Animals* (*31*).

PET

All PET scans were obtained using a microPET Focus 220 (Siemens) scanner designed for laboratory animals. Monkeys were sedated with ketamine (5 mg/kg, intramuscularly) combined with atropine hydrosulfate (0.08 mg/kg) and anesthetized with a continuous intravenous infusion of propofol (10 mg/kg/h). Monkeys were immobilized with a head-fixation device to ensure the accuracy of repositioning throughout PET scanning. During anesthesia, heart rate (electrocardiogram), body temperature, and oxygen saturation were monitored. Oxygen gas was administered through the nasal cannula throughout the study to maintain oxygen saturation. Before emission scans, the animal's head was placed near the center of the PET camera's field of view, and transmission scans with a rotating ^{68}Ge/^{68}Ga pin source were acquired for 30 min for reproduction of the brain positioning and attenuation correction.

At the start of the emission scan, *R*-^{11}C-verapamil or ^{11}C-oseltamivir was administered via the saphenous vein as a single bolus, and then saline was flushed into the catheter line to prevent radiotracer adsorption or retention. The injected doses of *R*-^{11}C-verapamil and ^{11}C-oseltamivir were 66 ± 19 and 77 ± 13 MBq/kg, respectively. Both PET scans were obtained in the same day. A dynamic emission scan in 3-dimensional list-mode was obtained for 60 min, and a total of 25 frames were collected in the following manner: 12 × 10, 6 × 30, 3 × 300, and 4 × 600 s. A matched MR image of the brain was obtained before or after the PET scan within 2 wk for infant and adolescent monkeys and within 4 wk for adult monkeys. After drug administration, arterial blood (~0.5–1.5 mL) was sampled via an indwelling arterial port in the saphenous artery at the following times: 0.5, 1, 1.5, 2, 2.5, 4, 10, 20, 40, and 60 min (for infant and adolescent animals), and 8, 16, 24, 32, 40, 48, and 56 s and 1.1, 1.5, 2.5, 4, 10, 20, 30, and 60 min (for adults). The different blood sampling intervals

for the younger and adult animals were used to limit the total volume of blood collected to no more than 5.6 mL/kg of body weight. Sampling intervals were designed so they did not influence the outcome parameter of integration plot analysis. Blood radioactivity was counted in a 1470 Wizard Automatic γ-Counter (PerkinElmer), and the radioactivity in each sample was corrected for time decay from the point of radiotracer administration.

Metabolite Analysis

R-^{11}C-verapamil blood metabolites were analyzed at 1, 4, and 20 min. Arterial blood was deproteinized by adding an equivalent volume of acetonitrile, followed by centrifugation at 12,000 rpm for 2 min at 4°C. *R*-^{11}C-verapamil and its metabolites were analyzed in the supernatant using a high-performance liquid chromatograph (Shimadzu Corp.) coupled to a NaI(Tl) positron detector (UG-SCA30; Universal Giken). Components were separated on a Luna C18 column (30 mm × 4.6 mm, 5 μm; Phenomenex Inc.) at a flow rate of 2.5 mL/min. The initial solvent conditions were acetonitrile:water (31:69, v/v) containing 10 mM ammonium acetate (pH 7.2). After a 0.2-min sample injection, the ratio of acetonitrile:water was changed to 80:20 (v/v) in a linear fashion over 2.3 min and maintained at 80:20 for 0.4 min. The column was then washed using initial solvent conditions. The amount of intact *R*-^{11}C-verapamil was calculated as a percentage of the total amount of radioactivity.

Blood metabolites were analyzed at 1, 4, 10, 20, and 30 min after administration of ^{11}C-oseltamivir. Arterial blood was deproteinized by adding an equivalent volume of acetonitrile, followed by centrifugation at 12,000 rpm for 2 min at 4°C. Each supernatant was applied to a RP-8 thin-layer chromatography plate (Merck), which was developed with an acetonitrile:water:formic acid (10:10:0.1) mobile phase. After migration, each plate was dried and exposed to BAS TR2040 imaging plates (Fuji Film). The distribution of radioactivity on the imaging plates was determined by digital photostimulated luminescence autoradiography using a FLA-7000 analyzer (Fuji Film).

Analysis of PET Data

PET images were reconstructed using microPET Manager (Siemens) and the following parameters: standard 2-dimensional filtered backprojection using a Hanning filter with cutoff of 0.4 cycles per pixel. A volume of interest was made from related regions of interest, which were delineated in 1 slice on the basis of the corresponding brain MR image using the PMOD 3.0 program (PMOD Technologies Inc.). For each volume of interest, the decay-corrected time-radioactivity was normalized to the injected dose (% dose) to construct time–radioactivity curves.

Kinetic Analysis

Initial uptake rates for each brain region were calculated by the integration plot method (*32*), identical to Patlak plot method (*33,34*), using time–radioactivity curves for short periods (0.5–2.5 min after administration), during which the effect of *R*-^{11}C-verapamil or ^{11}C-oseltamivir metabolism was negligible. The radiotracer uptake rate was obtained using Equation 1:

$$\frac{X_{t\_tissue}}{C_{t\_blood}} = CL_{uptake\_tissue} \times \frac{AUC_{0\text{-}t}}{C_{t\_blood}} + V_{E,brain} \qquad \text{Eq. 1}$$

where CL_{uptake_tissue} is the brain tissue uptake clearance based on intact blood radiotracer. X_{t_tissue} represents the amount of ^{11}C radioactivity in brain tissue at time *t*, $AUC_{0\text{-}t}$ the area under the blood concentration–time curve from time 0 to time t, and C_{t_blood} the blood concentration at time *t* calculated from intact radiotracer. $V_{E,brain}$ represents the initial distribution volume in brain tissue at time 0, calculated from the *y*-intercept of the integration plot. The CL_{uptake_tissue} value can be obtained from the initial slope of a plot of X_{t_tissue}/C_{t_blood} versus $AUC_{0\text{-}t}/C_{t\_blood}$.

Statistical Analysis

Data are presented as the mean ± SD for 5 monkeys in the *R*-^{11}C-verapamil study and the individual data for 2 monkeys in the ^{11}C-oseltamivir study. When appropriate, significant differences between groups were identified using the Student 2-tailed unpaired *t* test and 1-way ANOVA, followed by Bonferroni's multiple-comparison procedure. Two-way ANOVA was used to test for differences in the ratio of brain concentration to blood concentration ($K_{p,brain}$) among the groups. Statistical significance was set at a p value less than 0.05.

RESULTS

Distribution of *R*-^{11}C-Verapamil and ^{11}C-Oseltamivir Radioactivity in Infant, Adolescent, and Adult Monkey Brains

Figure 1 shows typical PET brain images of the distribution of *R*-^{11}C-verapamil or ^{11}C-oseltamivir and corresponding morphologic MR images of infant (age, 9 mo) and adult (age, 6.5 y) monkeys. The uptake of ^{11}C radioactivity after *R*-^{11}C-verapamil or ^{11}C-oseltamivir administration was higher in the brain of infants than in adults, although no adverse event was observed during and after the PET studies using both radiotracers. The highest uptake of both radiotracers was observed in the lateral and third ventricles, including the choroid plexus, of both infants and adults.

Time–radioactivity curves for *R*-^{11}C-verapamil in the brain of infant, adolescent, and adult monkeys are shown in Figure 2A. In all animals, the amount of ^{11}C radioactivity

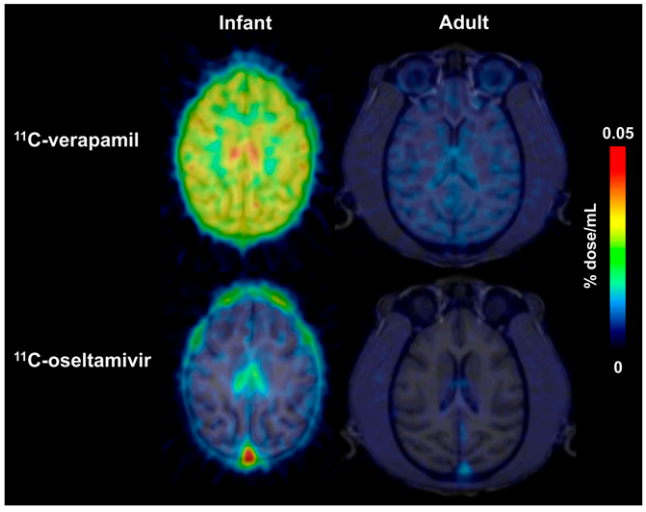

FIGURE 1. Color-coded fusion images of horizontal slices of summated PET images from 0.5 to 2.5 min and corresponding brain MRI scans for infant and adult monkey after administration of *R*-^{11}C-verapamil or ^{11}C-oseltamivir.

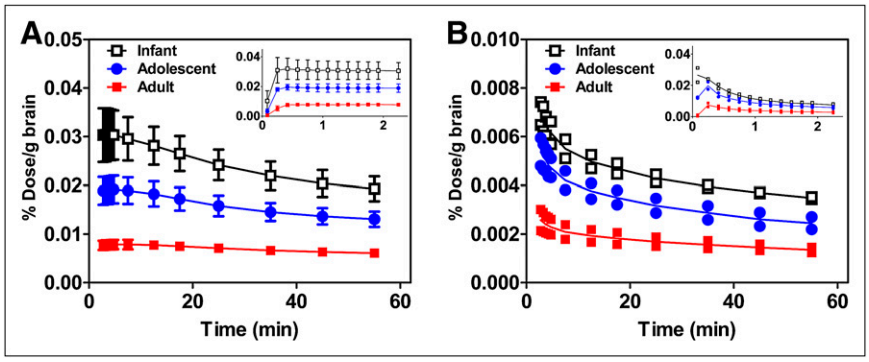

FIGURE 2. Time–radioactivity curves for monkey brains after intravenous administration of *R*-^{11}C-verapamil (A) or ^{11}C-oseltamivir (B). Time profiles of radioactivity distribution in brains of rhesus monkeys were determined using PET during a 60-min period after radiotracer administration. Insets show curve detail in early time period (up to 2.5 min). Each data point represents mean ± SD (n = 5) for *R*-^{11}C-verapamil–administered group and individual data of two ^{11}C-oseltamivir–administered monkeys.

in the brain peaked at 0.25–4.3 min after intravenous administration of *R*-^{11}C-verapamil. The maximum brain concentration ($C_{max,brain}$) in infants, adolescents, and adults was 0.033 ± 0.007, 0.020 ± 0.002, and 0.0082% ± 0.0007% dose/g of brain, respectively. The $C_{max,brain}$ was significantly higher in the infant and adolescent groups than in the adult group (4.1-fold higher in infants and 2.5-fold higher in adolescents, Table 1, $p < 0.05$). The ^{11}C radioactivity in the brain of adults remained constant at approximately 0.0077% dose/g until 60 min, whereas ^{11}C radioactivity in the brain of infants and adolescents gradually decreased for 60 min. The brain area under the curve (AUC_{brain}) from 0 to 2.5 min was 0.081% ± 0.017% dose × min/g for the infant group, 0.049% ± 0.007% dose × min/g for the adolescent group, and 0.020% ± 0.002% dose × min/g for the adult group (Table 1).

Time–radioactivity curves for ^{11}C-oseltamivir in the brains of infant, adolescent, and adult monkeys revealed that ^{11}C radioactivity peaked in all groups within 0.25 min, rapidly decreased for 10 min, then gradually decreased until 60 min after intravenous administration (Fig. 2B). The $C_{max,brain}$ was 0.024% and 0.031% for infants, 0.017% and 0.022% for adolescents, and 0.0062% and 0.0086% dose/g for adults (Table 1). The AUC_{brain} from 0 to 2.5 min was 0.030% and 0.034% dose × min/g in the infant group, 0.021% and 0.026% dose × min/g in the adolescent group, and 0.0082% and 0.012% dose × min/g in the adult group (Table 1). There was a tendency toward a lower $C_{max,brain}$ and AUC_{brain} in the adult group; however, the differences were smaller than those observed in the *R*-^{11}C-verapamil study.

Metabolism and Time–Radioactivity Profiles for *R*-^{11}C-Verapamil and ^{11}C-Oseltamivir in Arterial Blood

A radiochromatogram high-performance liquid chromatography analysis of *R*-^{11}C-verapamil in arterial blood was performed to determine the plasma concentration of intact *R*-^{11}C-verapamil. The retention time of intact *R*-^{11}C-verapamil was approximately 2.4 min, and that of its major metabolite was 0.5 min (Supplemental Fig. 1A; supplemental materials are available online only at http://jnm.

TABLE 1
Pharmacokinetic Parameters of *R*-^{11}C-Verapamil and ^{11}C-Oseltamivir After Intravenous Administration.

Pharmacokinetic parameter	Infant (9 mo)	Adolescent (24–27 mo)	Adult (5.5–6.8 y)
R-^{11}C-verapamil			
$C_{max,brain}$ (% dose/mL)	0.033 ± 0.007*	0.020 ± 0.002†	0.0082 ± 0.0007
$T_{max,\ brain}$ (min)	1.9 ± 2.2	1.6 ± 1.8	2.2 ± 2.4
$CL_{uptake,brain}$ (mL/min/g)	0.14 ± 0.04†	0.087 ± 0.023	0.061 ± 0.011
$V_{E,brain}$ (mL/g brain)	0.12 ± 0.03‡	0.069 ± 0.019*	0.048 ± 0.008
$AUC_{brain,0–2.5\ min}$ (% dose × min/g)§	0.081 ± 0.017	0.049 ± 0.007	0.020 ± 0.002
$AUC_{blood,0–2.5\ min}$ (% dose × min/mL)	0.23 ± 0.10	0.20 ± 0.07	0.10 ± 0.01
^{11}C-oseltamivir			
$C_{max,brain}$ (% dose/mL)	0.024, 0.031	0.017, 0.022	0.0062, 0.0086
$T_{max,\ brain}$ (min)	0.083, 0.25	0.25, 0.25	0.25, 0.25
$CL_{uptake,brain}$ (mL/min/g)	0.0097, 0.0104	0.0097, 0.0098	0.0072, 0.0079
$V_{E,brain}$ (mL/g)	0.024, 0.031	0.026, 0.030	0.019, 0.024
$AUC_{brain,0–2.5\ min}$ (% dose × min/g)	0.030, 0.034	0.021, 0.026	0.0082, 0.012
$AUC_{blood,0–2.5\ min}$ (% dose × min/mL)	0.49, 0.67	0.37, 0.50	0.26, 0.30

*Statistically significant age-related difference was observed for some pharmacokinetic parameters (unpaired t test, $p < 0.05$).
†Statistically significant age-related difference was observed for some pharmacokinetic parameters (unpaired t test, $p < 0.001$).
‡Statistically significant age-related difference was observed for some pharmacokinetic parameters (unpaired t test, $p < 0.01$).
§A significant age-related difference in AUC_{brain} ($p < 0.05$, 1-way ANOVA, Bonferroni's multiple-comparison procedure) was observed.
$CL_{uptake,brain}$ and $V_{E,brain}$ were obtained by integration plot analysis using Equation 1.

snmjournals.org). By 4 min after *R*-^{11}C-verapamil administration, radioactivity associated with the *R*-^{11}C-verapamil metabolite in the arterial plasma of infants, adolescents, and adults was approximately 15%, 30%, and 10% of the total radioactivity, respectively (Fig. 3A). Approximately 80% of plasma radioactivity was associated with the *R*-^{11}C-verapamil metabolite by 30 min after administration.

Figure 3B shows time–radioactivity curves for intact *R*-^{11}C-verapamil in blood. In all groups, *R*-^{11}C-verapamil radioactivity fell sharply during the first 4 min after administration and then decreased gradually until 20 min. At all time points, blood radioactivity associated with intact *R*-^{11}C-verapamil was significantly higher in the infant and adolescent groups than in the adult group. The AUC of intact *R*-^{11}C-verapamil in blood from 0 to 2.5 min was 0.23% ± 0.10% dose × min/mL for the infant group, 0.20% ± 0.07% dose × min/mL for the adolescent group, and 0.10% ± 0.01% dose × min/mL for the adult group (Table 1).

Profiles of the ratio of brain concentration to blood concentration after administration of *R*-^{11}C-verapamil are shown in Figure 3C. The $K_{p,brain}$ for the infant group through 2.2 min was significantly higher than the $K_{p,brain}$ for both the adolescent and the adult groups (2-way ANOVA, $p < 0.05$). In addition, the AUC_{brain}-to-AUC_{blood} ratio was 2.3 ± 0.8-fold and 1.6 ± 0.5-fold higher in the infant and adolescent groups, respectively, than in the adult group.

Analysis of the thin-layer chromatography autoradiograms showed that a metabolite of ^{11}C-oseltamivir (^{11}C-Ro 64-0802) was found in the blood (Supplemental Fig. 1B). At 4 min after administration of ^{11}C-oseltamivir, radioactivity associated with ^{11}C-Ro 64-0802 was less than 3% of the total radioactivity in the arterial blood in all animals (Fig. 4A). ^{11}C-Ro 64-0802 radioactivity constituted approximately 30% of blood radioactivity by 20 min after administration. Radioactivity associated with intact ^{11}C-oseltamivir was higher in the infant and adolescent groups than in the adult group at all time points (Fig. 4B), and the $K_{p,brain}$ in the infant group through 2.2 min was slightly higher than in the adult group (Fig. 4C). The AUC_{brain}-to-AUC_{blood} ratios for the infant and adolescent groups were 1.4- to 1.7-fold and 1.4- to 1.6-fold higher, respectively, than for the adult group.

Brain Uptake Clearance of *R*-^{11}C-Verapamil or ^{11}C-Oseltamivir in Infant, Adolescent, and Adult Monkeys

Individual integration plots of *R*-^{11}C-verapamil or ^{11}C-oseltamivir brain uptake are shown in Figure 5. The plots showed a clear linearity from 0.5 to 2.5 min after *R*-^{11}C-verapamil or ^{11}C-oseltamivir administration for all 3 groups. During this initial period, intact radiotracer and a small amount of metabolites accounted for more than 82% of ^{11}C radioactivity in the blood. To obtain a more accurate analysis, the $AUC_{0\text{-}t}$ and C_{t_blood} were calculated from the concentration of intact radiotracer in the blood. Because the brain volume per body weight for individual monkeys differed among age groups (44 ± 8 g/kg in infants, 32 ± 3 g/kg in adolescents, and 13 ± 4 g/kg in adults), we calculated the brain uptake clearance ($CL_{uptake,brain}$) on the basis of brain volume. The $CL_{uptake,brain}$ of *R*-^{11}C-verapamil (mL/min/g) was 0.061 ± 0.011 in the adult group, significantly lower than the $CL_{uptake,brain}$ in the infant (0.14 ± 0.04, $p < 0.01$) and adolescent (0.087 ± 0.023, $p = 0.06$) groups (Table 1). $V_{E,brain}$ values for *R*-^{11}C-verapamil (mL/g brain) in the infant, adolescent, and adult groups were 0.12 ± 0.03, 0.069 ± 0.019, and 0.048 ± 0.008, respectively. The ^{11}C-oseltamivir $CL_{uptake,brain}$ was 0.0072 and 0.0079 mL/min/g in the adult group, slightly lower than the $CL_{uptake,brain}$ in the infant (0.0097 and 0.0104 mL/min/g) and adolescent (0.0097

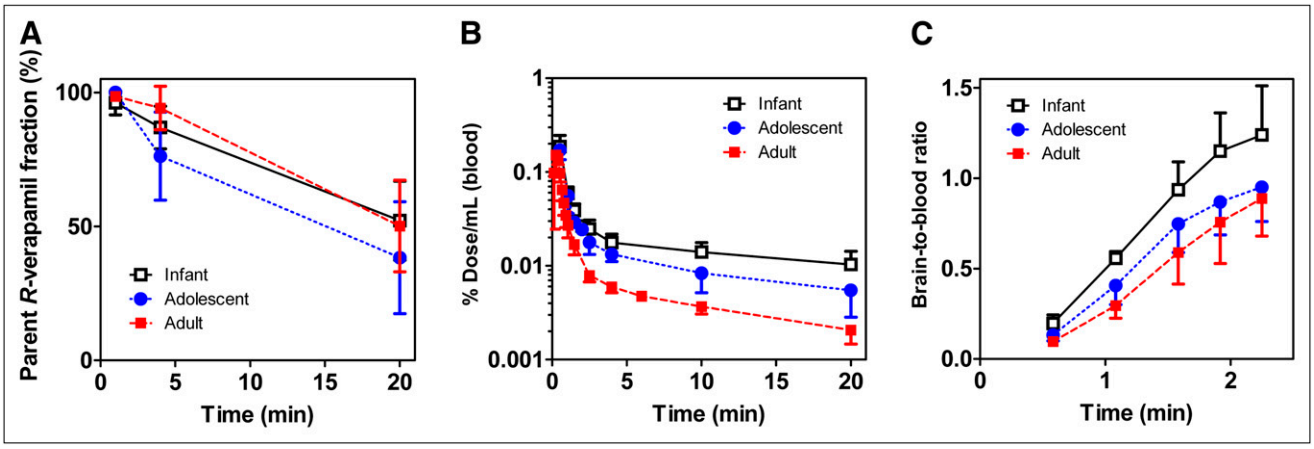

FIGURE 3. Intact radiotracer time–activity curves for monkey blood and ratio of brain radioactivity to blood radioactivity after intravenous administration of *R*-^{11}C-verapamil. (A) Fraction of blood radioactivity associated with intact *R*-^{11}C-verapamil. (B) Temporal distribution of intact *R*-verapamil in monkey blood determined by sampling blood at various intervals after administration of *R*-^{11}C-verapamil. (C) Ratio of brain radioactivity to blood intact *R*-verapamil activity was determined after administration of *R*-^{11}C-verapamil. Each data point represents mean ± SD ($n = 5$).

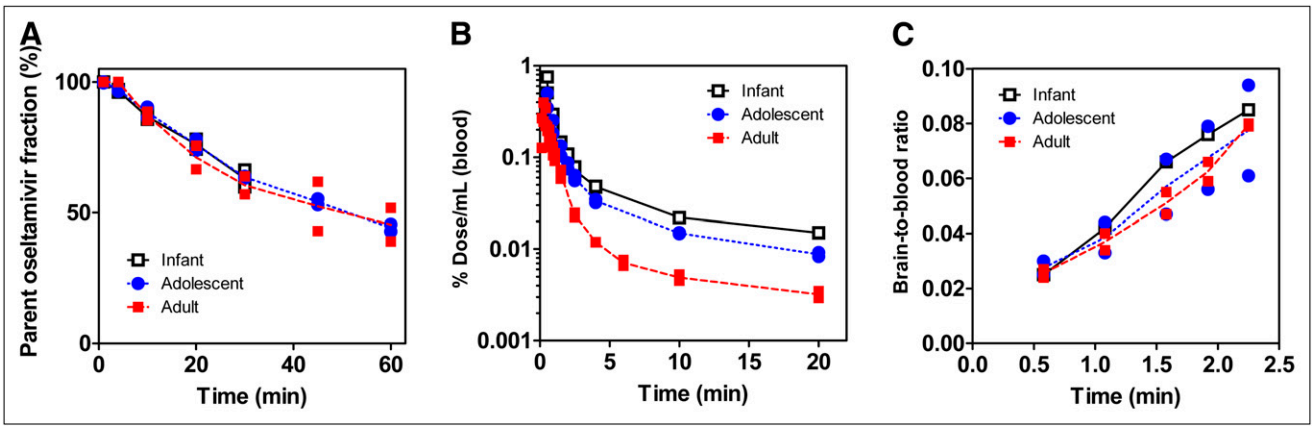

FIGURE 4. Metabolite analysis of monkey plasma, intact radiotracer time–activity curves for monkey blood, and ratio of brain radioactivity to blood radioactivity after intravenous administration of ^{11}C-oseltamivir. (A) Fraction of blood radioactivity associated with intact ^{11}C-oseltamivir. (B) Temporal distribution of intact oseltamivir in monkey blood determined by sampling blood at various intervals after administration of ^{11}C-oseltamivir. (C) Ratio of brain radioactivity to blood intact oseltamivir activity was determined after administration of ^{11}C-oseltamivir. Each data point represents individual data of 2 monkeys.

and 0.0098 mL/min/g) groups (Table 1). ^{11}C-oseltamivir $V_{E,brain}$ values (mL/g brain) were similar in the infant (0.024 and 0.031), adolescent (0.026 and 0.030), and adult (0.019 and 0.024) groups.

DISCUSSION

We examined developmental changes in P-gp function in the BBB of nonhuman primates by comparing the $CL_{uptake,brain}$ of *R*-^{11}C-verapamil and ^{11}C-oseltamivir to determine whether there were age-related differences in drug response in the CNS.

The *R*-^{11}C-verapamil AUC_{brain} and $C_{max,brain}$ were significantly higher in infants and adolescents than in adults (AUC_{brain}, 4.0- and 2.5-fold higher, respectively; $C_{max,brain}$, 4.1- and 2.5-fold higher, respectively). The ^{11}C-oseltamivir AUC_{brain} and $C_{max,brain}$ were also higher in infants and adolescents than in adults (AUC_{brain}, 4.1- and 2.3-fold higher, respectively; $C_{max,brain}$, 3.7- and 2.7-fold higher, respectively). However, because the infant and adolescent AUC_{blood} values were also higher than the adult AUC_{blood} values (2.1- and 1.8-fold higher for verapamil and 1.6- and 1.5-fold higher for oseltamivir, respectively) (Fig. 4A), the greater AUC_{brain} and $C_{max,brain}$ values can be partially explained by greater systemic exposure. To exclude the effect of systemic exposure, we determined the $CL_{uptake,brain}$ for intact *R*-^{11}C-verapamil and ^{11}C-oseltamivir (the parameter disproportional to P-gp activity in the BBB (*21*)) using integration plot analysis. The initial slope of the plot was higher in the infant and adolescent groups than in the adult group after *R*-^{11}C-verapamil administration. Therefore, it is

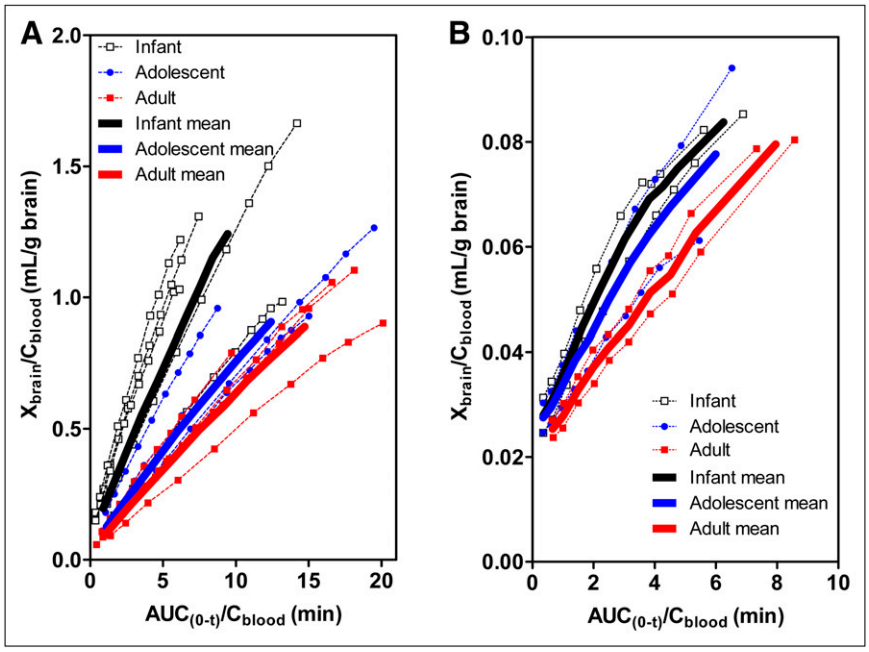

FIGURE 5. Individual integration plot of *R*-^{11}C-verapamil (A) or ^{11}C-oseltamivir (B) brain uptake in infant, adolescent, and adult monkeys.

most likely that P-gp expression increases with age in rhesus monkeys, as has been demonstrated in rats (*8*). Though the constant K_1 (influx rate constant from blood to brain) or V_d (the volume of distribution in the brain) value calculated by a simple 1-tissue-compartment model has been used for measuring P-gp function at the BBB, it required several time points for a longer term to get the reliable nonlinear fitting. In our study, we used integration plot analysis, which needs the data only in the initial periods (0.5–2.5 min), during which the amounts of the metabolites in plasma were small; the influence of the metabolites might be negligible. The additional study with P-gp inhibitors may further confirm P-gp function at the BBB; however, the study could not be performed in this case because of the risk for exposure to high doses of P-gp inhibitors in younger monkeys.

Consistent with results of the *R*-^{11}C-verapamil study, the ^{11}C-oseltamivir $CL_{uptake,brain}$ was higher in the infant and adolescent groups than in the adult group. The age-related differences in $CL_{uptake,brain}$ for ^{11}C-oseltamivir were unremarkable, compared with those for *R*-^{11}C-verapamil, presumably because of ^{11}C-oseltamivir's low BBB permeability derived from its low lipophilicity. To our knowledge, this study demonstrates for the first time age-associated developmental changes in P-gp function in the BBB in rhesus monkeys, using a noninvasive in vivo brain imaging technique. Using immunohistochemical analyses of infant and adult human postmortem brain samples, Daood et al. (*35*) reported that CNS P-gp expression increases during development. Combined with *R*-^{11}C-verapamil PET analyses that showed that cerebral P-gp function decreases in older adults, these results suggested that human P-gp function in the BBB should also change with age (*36*). Therefore, it is possible that infant and adolescent brains are more sensitive to the pharmacologic and adverse effects of P-gp substrates than are adult brains, even though the systemic exposure is similar.

Ours is also the first study examining the brain penetration of ^{11}C-oseltamivir in nonhuman primates. Hatori et al. (*37*) examined the disposition of ^{11}C-oseltamivir in adult mice, but the brain concentration of ^{11}C-oseltamivir was below the limit of detection. Conversion of ^{11}C-oseltamivir to ^{11}C-Ro 64-0802 by carboxy esterase occurs more rapidly in adult mice than in adult monkeys, primarily because of differences in carboxy esterase activity in mouse and monkey serum. Therefore, the lower brain to blood concentration ratio of ^{11}C-oseltamivir in mice than in primates makes the nonhuman primate a better model for predicting how developmental changes affect the penetration of oseltamivir into the brain of humans.

The differences in ^{11}C-oseltamivir $CL_{uptake,brain}$ and blood concentration between younger and adult animals in our study may partially explain the safety data in oseltamivir medication. We focused on oseltamivir; however, Ro 64-0802 is the major metabolite and is an active form of the drug that also penetrates the brain in mice with a low permeability, due to active efflux mediated by MRP4 (*37,38*). Ro 64-0802 is more potent than oseltamivir and causes neuronal excitability in rat hippocampal slices (*39*). Therefore, developmental changes in MRP4 activity should also be investigated.

The plasma concentrations of intact *R*-^{11}C-verapamil and ^{11}C-oseltamivir were slightly higher in younger monkeys than in adults. Because verapamil and oseltamivir systemic exposure depends on the activity of cytochrome P-450 and carboxy esterase, these data indicate that metabolic enzymes may show developmental changes. Strolin et al. (*40*) reported that age-related differences in the expression of some phase I and phase II enzymes do exist in humans, and Ose et al. (*8*) reported that conversion activity in newborn rat plasma and S9 specimens is lower than in adults. Developmental changes in metabolism may have a greater impact on the response to drugs in younger subjects. Because P-gp is also expressed in the liver and small intestine, developmental changes in P-gp expression in these organs will cause age-related differences in the systemic exposure of P-gp substrates. Schuetz et al. (*41*) reported that *MDR1* messenger RNA in human pediatric livers is undetectable and suggested that P-gp expression appears to be developmentally regulated in the liver. However, such information is not available regarding P-gp expression in the small intestine.

CONCLUSION

This study examined age-related developmental changes in P-gp function in the BBB in nonhuman primates using in vivo *R*-^{11}C-verapamil PET. The clearance of brain *R*-^{11}C-verapamil uptake was significantly greater in younger monkeys than in adults, indicating that P-gp function in the BBB is immature in infant and adolescent monkeys. In addition, the PET study showed that brain penetration of ^{11}C-oseltamivir changed with development and was slightly higher in younger monkeys.

DISCLOSURE STATEMENT

The costs of publication of this article were defrayed in part by the payment of page charges. Therefore, and solely to indicate this fact, this article is hereby marked "advertisement" in accordance with 18 USC section 1734.

ACKNOWLEDGMENTS

We are indebted to Akihiro Kawasaki, Chiho Takeda, Yumiko Katayama, and Emi Hayashinaka for their expert technical assistance. This study was supported in part by a consignment expense from the Molecular Imaging Program on "Research Base for Exploring New Drugs" from the Ministry of Education, Culture, Sports, Science, and Technology (MEXT), Government of Japan.

REFERENCES

1. Alcorn J, McNamara PJ. Using ontogeny information to build predictive models for drug elimination. *Drug Discov Today.* 2008;13:507–512.
2. Blake MJ, Castro L, Leeder JS, Kearns GL. Ontogeny of drug metabolizing enzymes in the neonate. *Semin Fetal Neonatal Med.* 2005;10:123–138.

3. Kearns GL, Leeder JS, Gaedigk A. Impact of the CYP2C19*17 allele on the pharmacokinetics of omeprazole and pantoprazole in children: evidence for a differential effect. *Drug Metab Dispos.* 2010;38:894–897.
4. Kusuhara H, Sugiyama Y. Active efflux across the blood-brain barrier: role of the solute carrier family. *NeuroRx.* 2005;2:73–85.
5. Pardridge WM. The blood-brain barrier: bottleneck in brain drug development. *NeuroRx.* 2005;2:3–14.
6. Nitta T, Hata M, Gotoh S, et al. Size-selective loosening of the blood-brain barrier in claudin-5-deficient mice. *J Cell Biol.* 2003;161:653–660.
7. Goralski KB, Acott PD, Fraser AD, Worth D, Sinal CJ. Brain cyclosporin A levels are determined by ontogenic regulation of mdr1a expression. *Drug Metab Dispos.* 2006;34:288–295.
8. Ose A, Kusuhara H, Yamatsugu K, et al. P-glycoprotein restricts the penetration of oseltamivir across the blood-brain barrier. *Drug Metab Dispos.* 2008;36:427–434.
9. Tamai I, Tsuji A. Transporter-mediated permeation of drugs across the blood-brain barrier. *J Pharm Sci.* 2000;89:1371–1388.
10. Kusuhara H, Sugiyama Y. Efflux transport systems for drugs at the blood-brain barrier and blood-cerebrospinal fluid barrier (part 1). *Drug Discov Today.* 2001;6:150–156.
11. Schinkel AH, Wagenaar E, van Deemter L, Mol CA, Borst P. Absence of the mdr1a P-glycoprotein in mice affects tissue distribution and pharmacokinetics of dexamethasone, digoxin, and cyclosporin A. *J Clin Invest.* 1995;96:1698–1705.
12. Kim RB, Fromm MF, Wandel C, et al. The drug transporter P-glycoprotein limits oral absorption and brain entry of HIV-1 protease inhibitors. *J Clin Invest.* 1998;101:289–294.
13. Mealey KL, Bentjen SA, Gay JM, Cantor GH. Ivermectin sensitivity in collies is associated with a deletion mutation of the mdr1 gene. *Pharmacogenetics.* 2001; 11:727–733.
14. Mealey KL, Northrup NC, Bentjen SA. Increased toxicity of P-glycoprotein-substrate chemotherapeutic agents in a dog with the MDR1 deletion mutation associated with ivermectin sensitivity. *J Am Vet Med Assoc.* 2003;223:1453–1455, 1434.
15. Lagas JS, van Waterschoot RA, van Tilburg VA, et al. Brain accumulation of dasatinib is restricted by P-glycoprotein (ABCB1) and breast cancer resistance protein (ABCG2) and can be enhanced by elacridar treatment. *Clin Cancer Res.* 2009;15:2344–2351.
16. Sadeque AJ, Wandel C, He H, Shah S, Wood AJ. Increased drug delivery to the brain by P-glycoprotein inhibition. *Clin Pharmacol Ther.* 2000;68:231–237.
17. Pankaj JP. Treatment of disorders of bowel motility and water flux. InGilman AG, Goodman LS, Laurence LB, John SL, Keith LP, eds. *The Pharmacological Basis of Therapeutics*. 11th ed. New York, NY: McGraw-Hill Company; 2006:983–1008.
18. Luurtsema G, Molthoff CF, Windhorst AD, et al. (*R*)- and (*S*)-[^{11}C]verapamil as PET-tracers for measuring P-glycoprotein function: in vitro and in vivo evaluation. *Nucl Med Biol.* 2003;30:747–751.
19. Lee YJ, Maeda J, Kusuhara H, et al. In vivo evaluation of P-glycoprotein function at the blood-brain barrier in nonhuman primates using [^{11}C]verapamil. *J Pharmacol Exp Ther.* 2006;316:647–653.
20. Lubberink M, Luurtsema G, van Berckel BN, et al. Evaluation of tracer kinetic models for quantification of P-glycoprotein function using (*R*)-[^{11}C]verapamil and PET. *J Cereb Blood Flow Metab.* 2007;27:424–433.
21. Sasongko L, Link JM, Muzi M, et al. Imaging P-glycoprotein transport activity at the human blood-brain barrier with positron emission tomography. *Clin Pharmacol Ther.* 2005;77:503–514.
22. Takano A, Kusuhara H, Suhara T, et al. Evaluation of in vivo P-glycoprotein function at the blood-brain barrier among MDR1 gene polymorphisms by using ^{11}C-verapamil. *J Nucl Med.* 2006;47:1427–1433.
23. Bartels AL, Willemsen AT, Kortekaas R, et al. Decreased blood-brain barrier P-glycoprotein function in the progression of Parkinson's disease, PSP and MSA. *J Neural Transm.* 2008;115:1001–1009.
24. Echizen H, Brecht T, Niedergesass S, Vogelgesang B, Eichelbaum M. The effect of dextro-, levo-, and racemic verapamil on atrioventricular conduction in humans. *Am Heart J.* 1985;109:210–217.
25. Chung FS, Eyal S, Muzi M, et al. Positron emission tomography imaging of tissue P-glycoprotein activity during pregnancy in the non-human primate. *Br J Pharmacol.* 2010;159:394–404.
26. Eyal S, Chung FS, Muzi M, et al. Simultaneous PET imaging of P-glycoprotein inhibition in multiple tissues in the pregnant nonhuman primate. *J Nucl Med.* 2009;50:798–806.
27. Syvanen S, Hammarlund-Udenaes M. Using PET studies of P-gp function to elucidate mechanisms underlying the disposition of drugs. *Curr Top Med Chem.* 2010; 10:1799–1809.
28. Toovey S, Rayner C, Prinssen E, et al. Assessment of neuropsychiatric adverse events in influenza patients treated with oseltamivir: a comprehensive review. *Drug Saf.* 2008;31:1097–1114.
29. Morita M, Sone T, Yamatsugu K, et al. A method for the synthesis of an oseltamivir PET tracer. *Bioorg Med Chem Lett.* 2008;18:600–602.
30. Wegman TD, Maas B, Elsinga PH, Vaalburg W. An improved method for the preparation of [^{11}C]verapamil. *Appl Radiat Isot.* 2002;57:505–507.
31. *Guide for the Care and Use of Laboratory Animals*. Bethesda, MD: National Institutes of Health; 1985. NIH publication 85-23.
32. Kim DC, Sugiyama Y, Satoh H, Fuwa T, Iga T, Hanano M. Kinetic analysis of in vivo receptor-dependent binding of human epidermal growth factor by rat tissues. *J Pharm Sci.* 1988;77:200–207.
33. Patlak CS, Blasberg RG. Graphical evaluation of blood-to-brain transfer constants from multiple-time uptake data. Generalizations. *J Cereb Blood Flow Metab.* 1985;5:584–590.
34. Mankoff DA, Shields AF, Graham MM, Link JM, Krohn KA. A graphical analysis method to estimate blood-to-tissue transfer constants for tracers with labeled metabolites. *J Nucl Med.* 1996;37:2049–2057.
35. Daood M, Tsai C, Ahdab-Barmada M, Watchko JF. ABC transporter (P-gp/ABCB1, MRP1/ABCC1, BCRP/ABCG2) expression in the developing human CNS. *Neuropediatrics.* 2008;39:211–218.
36. Unadkat JD, Chung F, Sasongko L, et al. Rapid solid-phase extraction method to quantify [^{11}C]-verapamil, and its [^{11}C]-metabolites, in human and macaque plasma. *Nucl Med Biol.* 2008;35:911–917.
37. Hatori A, Arai T, Yanamoto K, et al. Biodistribution and metabolism of the anti-influenza drug [^{11}C]oseltamivir and its active metabolite [^{11}C]Ro 64-0802 in mice. *Nucl Med Biol.* 2009;36:47–55.
38. Ose A, Ito M, Kusuhara H, et al. Limited brain distribution of [3R,4R,5S]-4-acetamido-5-amino-3-(1-ethylpropoxy)-1-cyclohexene-1-carboxylate phosphate (Ro 64-0802), a pharmacologically active form of oseltamivir, by active efflux across the blood-brain barrier mediated by organic anion transporter 3 (Oat3/Slc22a8) and multidrug resistance-associated protein 4 (Mrp4/Abcc4). *Drug Metab Dispos.* 2009;37:315–321.
39. Izumi Y, Tokuda K, O'Dell KA, Zorumski CF, Narahashi T. Neuroexcitatory actions of Tamiflu and its carboxylate metabolite. *Neurosci Lett.* 2007;426:54–58.
40. Strolin Benedetti M, Whomsley R, Baltes EL. Differences in absorption, distribution, metabolism and excretion of xenobiotics between the paediatric and adult populations. *Expert Opin Drug Metab Toxicol.* 2005;1:447–471.
41. Schuetz EG, Furuya KN, Schuetz JD. Interindividual variation in expression of P-glycoprotein in normal human liver and secondary hepatic neoplasms. *J Pharmacol Exp Ther.* 1995;275:1011–1018.